PROCEEDINGS OF SPIE

SPIEDigitalLibrary.org/conference-proceedings-of-spie

Towards combined multispectral, FLIM and Raman imaging for skin diagnostics

Spigulis, J., Kuzmina, I., Lukinsone, V., Tamošiūnas, M., Oshina, I., et al.

J. Spigulis, I. Kuzmina, V. Lukinsone, M. Tamošiūnas, I. Oshina, L. Ozolina, A. Maslobojeva, M. Kuzminskis, D. Ivanov, E. Borisova, "Towards combined multispectral, FLIM and Raman imaging for skin diagnostics," Proc. SPIE 11232, Multimodal Biomedical Imaging XV, 112320N (17 February 2020); doi: 10.1117/12.2559107

SPIE.

Event: SPIE BiOS, 2020, San Francisco, California, United States

Towards combined multispectral, FLIM and Raman imaging for skin diagnostics

J.Spigulis[1]*, I.Kuzmina[1], V.Lukinsone[1], M.Tamošiūnas[1], I.Oshina[1], L.Ozolina[1], A.Maslobojeva[1], M.Kuzminskis[1], D.Ivanov[2], E.Borisova[2]

[1)] Biophotonics Laboratory, Institute of Atomic Physics and Spectroscopy, University of Latvia
Raina Blvd. 19, Riga, LV-1586, Latvia
[2)] Institute of Electronics, Bulgarian Academy of Sciences, 72 Tsarigradsko chaussee Blvd., 1784 Sofia, Bulgaria

ABSTRACT

To explore challenges for further improvement of diagnostic performance, a project aimed at development of technology for tri-modal skin imaging by combining multispectral, fluorescence lifetime and Raman band imaging was initiated. In this study, each of the mentioned imaging modalities has been preliminary tested and updated. Four different multispectral imaging devices were tested on color standards. Picosecond laser-excited fluorescence lifetime imaging equipment was examined on *ex-vivo* skin samples. Finally, a new Raman spectroscopy setup with 785 nm laser was launched and tested on cell cultures and *ex-vivo* skin. Advantages and specific features of the tri-modal skin imaging are discussed.

Keywords: Multimodal biomedical imaging, optical skin diagnostics, fluorescence lifetime, Raman spectroscopy.

1. INTRODUCTION

Optical skin diagnostics is often a combination of different imaging/spectroscopy modalities. Recent studies confirmed that single imaging modality cannot ensure reliable non-contact diagnostics of skin malformations, including skin cancers; bi-modal multispectral and fluorescent imaging approach has led to much higher sensitivity and specificity[1]. To enhance the diagnostic accuracy, Raman spectroscopy has been successfully combined with autofluorescence based diagnostic techniques. The study by Zakharov et al.[2] showed that Raman and steady state autofluorescence spectroscopy could be easily integrated into a single optical device enabling the identification of malignant melanoma *ex vivo* with 100 % sensitivity of and 94 % specificity. More recent work by the same group tested the combination of Raman spectroscopy with NIR-VIS autofluorescence spectroscopy at clinical conditions[3]. It was demonstrated that Raman measurements alone were able to discriminate between MM and BCC with 97 % sensitivity and 62 % specificity. Additional criteria for VIS-NIR autofluorescence have increased the sensitivity and specificity between MM and BCC separation *ex vivo* to 100 % and 96 %, respectively[3]. Single cell experiments also showed that combined Raman scattering and autofluorescence signals can be employed to detect changes in cell metabolism during the MCF-7 cell differentiation stimulated by heregulin[4].

The first study for Raman spectroscopy and autofluorescence lifetime techniques combination was published by Dochow et al.[5] In this study, optical signals, co-acquired in situ using Raman and fluorescence lifetime spectroscopy techniques, were coupled to specific fiber optical probe for single point measurements or to create a 2D images of bone, fat, muscle, brain and blood vessels by using the raster scanning. The study revealed correlation of fluorescence lifetime and Raman spectroscopy data suggesting possibility to identify specific biochemical, morphological and structural features within the biological tissue samples. The application of fluorescence lifetime-guided acquisition of Raman spectra was extended to characterize human coronary arteries plaque composition *ex vivo*[6]. Depth resolved information was possible to acquire employing the multi-modal approach: fluorescence lifetime detected collagen, elastin, lipid and macrophages presence in the upper layers of lesion and Raman spectroscopy detected triglycerides, cholesterol, carotenoids and calcium molecules at ~700 micron depth for plaque chemical characterization. The relevant experiments with integrated FLIM confocal microscopy and Raman microscopy set-up were also carried in *Arabidopsis thaliana* plant models[7]. Differences in the biochemical specificity between *wt* (wild type) and *cad* mutants produced both the shift in autofluorescence lifetime and Raman spectra alterations.

*) janis.spigulis@lu.lv

Multimodal Biomedical Imaging XV, edited by Fred S. Azar, Xavier Intes, Qianqian Fang, Proc. of SPIE
Vol. 11232, 112320N · © 2020 SPIE · CCC code: 1605-7422/20/$21 · doi: 10.1117/12.2559107

Majumder[8] investigated the utility of combining Raman spectroscopy, autofluorescence and diffuse reflectance spectroscopy techniques for characterization of human breast pathologies. The performance metrics of elaborated diagnostic algorithms (HTM) was in the order of increased efficacy: autofluorescence (0.83), diffuse reflectance (0.88) and Raman spectroscopy (0.99). Although Raman spectral criteria were the most accurate for breast cancer diagnosis *ex vivo*, the combined Raman-autofluorescence and diffuse reflectance diagnostic algorithm could not classify the breast neoplastic transformations in a greater detail.

To explore challenges for further improvement of diagnostic performance, a three-year ERDF project aimed at development of technology for tri-modal skin imaging by combining multispectral, fluorescence lifetime and Raman band imaging was started in May, 2019. At its first stage, each of the above-mentioned imaging modalities has been laboratory-tested and updated. In particular, four different multispectral imaging devices (two of them - smartphone-based[9,10]) were tested on color standards. Picosecond laser-excited fluorescence lifetime imaging equipment[11] was tested on *ex- vivo* skin. Finally, a new Raman spectroscopy setup with 785 nm laser was launched and tested on cell samples and *ex vivo* skin. To our best knowledge, the skin malformations had been never investigated by combined Raman spectroscopy, autofluorescence lifetime and diffuse reflectance imaging techniques. Our study discusses the arguments to develop such tri-modal technique for improved diagnosis of skin malformations.

2. MATERIALS AND METHODS

2.1 Instrumentation

A comparative study of four multispectral skin imaging devices has been performed:

1. *Nuance EX* (commercial hyperspectral camera)[12],
2. *SkImager* (laboratory prototype)[13],
3. Smartphone *Nexus5* with RGB LED illuminator (laboratory prototype)[9],
4. Smartphone *Nexus5* with three wavelength laser illuminator (laboratory prototype)[10].

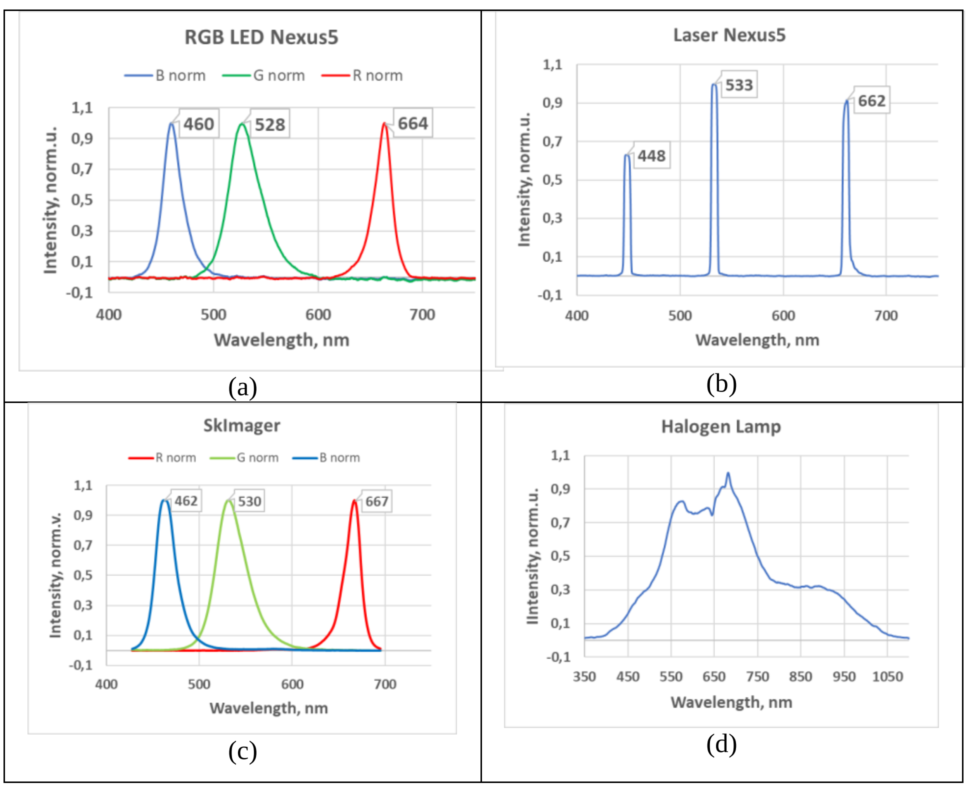

Fig.1. Normalized spectra of the light sources for multispectral imaging (halogen lamp - without detector sensitivity correction).

Table 1. Settings of the smartphone device cameras.

Device	**Nexus5+RGB LED**		**Nexus5+Laser**
Smartphone App	***AZ Camera***	***SkinViewer***	***AZ Camera***
ISO	100	100	100
Exposition time (s)			
t_R	0.08	0.02	0.25
t_G	0.06	0.02	0.25
t_B	0.04	0.02	0.25
Wavelength (nm)			
R	663		659
G	535		532
B	460		448

The *Nuance* camera was able to detect 51 spectral band images in the spectral range 450-950 nm at half-bandwidth ~10 nm. The spectral bands were selected by means of acousto-optical filter under broadband halogen lamp illumination. The other three devices used spectrally narrowband illumination; the corresponding spectra are presented on Fig.1.

Hyperspectral and RGB images were captured from 24 colour checker areas (*Xrite Color Checker Classic*). Settings of the smartphone-based devices are given in Table 1. Two smartphone applications – *AZ Camera* and *SkinViewer* - were used for image capturing by smartphone prototypes. *MatLab* software was used for the mean intensity readings from the manually selected regions of interest in the image.

The autofluorescence lifetime measurements were taken with ~200 ps time resolution using the SPC-150 TCSPC module (Becker&Hickl, Germany). The 405 nm laser 59 ps half-width pulses with 20 MHz repetition rate (LDH-D-C-405, PicoQuant, Germany) illuminated the sample *via* 200-μm silica core optical fiber with < 3 mW average power. Fluorescence was collected by a fiber bundle to the monochromator and transmitted at 460 nm or 520 nm wavelengths to the photon counting detector HPM-100-07 combined with detector controller DCC-100 (Becker&Hickl, Germany). The fast (τ_1) and slow (τ_2) lifetime components were calculated in frame of double-exponential decay model, and a double-mirror laser beam scanner was used for collection of the fluorescence lifetime images. The autofluorescence lifetime images were recorded as raster scans with a resolution of 312 μm in both x and y directions. Subsequently, lifetime data were visualized as pseudo color image. More details on the fluorescence lifetime imaging equipment can be found in[14].

The system for single-point Raman spectra acquisition was built around iHR320 (Horiba, Japan) spectrophotometer equipped with full chip vertically binned Sincerity CCD detector, filtered NIR laser excitation (Cobolt 08-NLD, 785 nm, line width 200 pm) and fiber bundle probe supplemented with 785 nm low pass filter and dichroic mirror (Edmund Optics). This was further combined with illumination and collection optics. Laser excitation at 75 mW power was focused to 0.08 cm^2 spot delivering up to 85 J/cm^2 fluency for single *in vitro* or *ex vivo* Raman spectroscopy measurement. All Raman data were baseline-corrected and analyzed in the 300 – 3100 cm^{-1} spectral interval.

2.2. Cell cultures and *ex vivo* tissue samples

Dc-3f murine cells suspension was initially maintained in tissue culture tube (TPP Techno Plastic Products AG, Switzerland) in DMEM (Sigma–Aldrich, St. Louis, MO, USA) supplemented with 10% fetal calf serum, 1% l-glutamine, 100 μg/ml streptomycin and 100 u./ml penicillin, up to 4 hours during the cells transportation. Before Raman measurements, the cells were re-suspended in PBS at 1.2×10^9 u./ml concentration, then pipetted vigorously and transferred (V = 50 μl) into a cylinder shaped and bottom flat container (h = 3mm; r = 2,5 mm) tightly covered inside with 24" gold folia. The fiber bundle comprising a single excitation fiber and 6 collection fibers (NA = 0.22) was positioned at 25 mm distance from the cell sample surface. Before conducting the Raman spectral measurements on the dead dc-3f cells, the cells were stored in PBS at 4 ^{o}C, for 1 week.

The human tissue *ex-vivo* samples in formalin were obtained from Dermatology Department, Queen Jiovanna—ISUL University Hospital, Sofia, Bulgaria. Based on histopathological evaluation, the tissues were classified as SCC skin cancer, BCC skin cancer, pigmented nevus and adjacent healthy skin. From each tissue sample, Raman spectra were taken at the central part of the lesion. During Raman spectra acquisition *ex vivo*, all samples were kept on a sheet of 24" gold folia. The samples were stored in formalin at 4^oC, therefore all Raman spectra *ex vivo* were subtracted by the reference spectra of formalin.

3. RESULTS AND DISCUSSION

3.1. Multispectral imaging

Full results of the comparative measurements of the multispectral imaging devices will be published elsewhere. To give sense about the main findings, Figures 2 and 3 illustrate the results for green channel at "green" illumination wavelengths of prototypes obtained for grey squares of the color checker. Similar results were obtained also for red and blue channels (not shown). The results of three prototypes for the settings experimentally adjusted for *in vivo* measurements in previous studies are shown in Fig.2(a, b). Smartphone-based devices show very similar mean intensity values for each grey scale square while *SkImager* gives higher intensity values compared to the smartphone-based devices (fig.2(a)). After normalization to the maximum value all three curves coincide (fig 2(b)). Fig.2(c, d) compare results obtained by smartphone RGB LED prototype at settings experimentally adjusted for *in vivo* measurements (*SkinViewer* App) with results obtained at settings adjusted for the color checker grey square (Ch20) using *Camera AZ* App. Figure 3 illustrates the difference of measured mean intensity values from reference values for three prototypes (fig.3(a)) and for two type of settings (experimentally selected for *in vivo* measurements and adjusted to the grey color checker square) of smartphone RGB LED prototype.

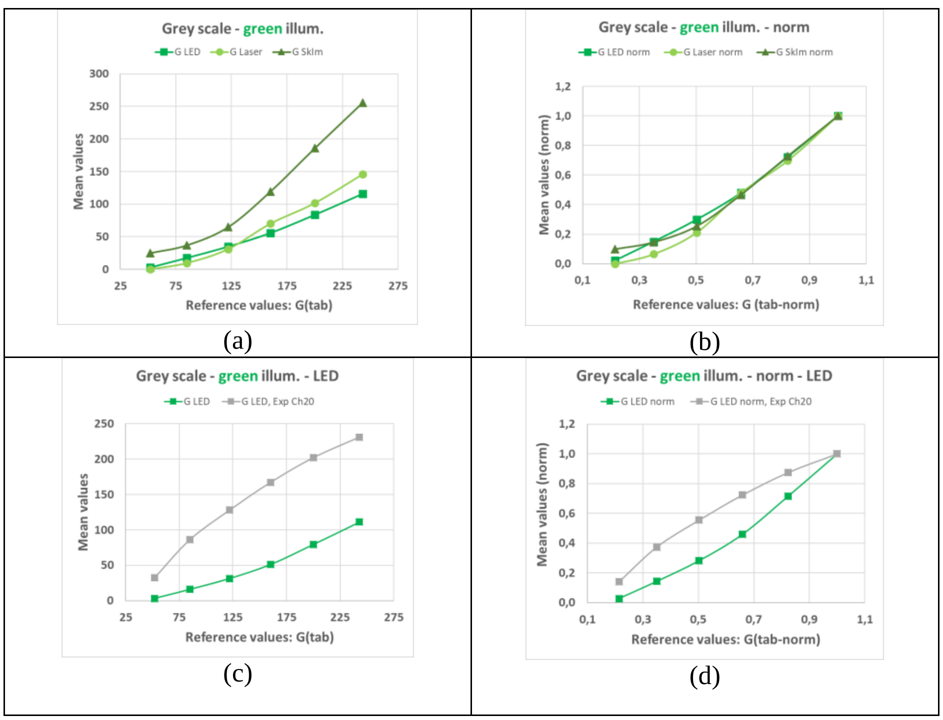

Fig.2. Dependences of the mean (a,c) and normalized (b,d) values on the reference values for grey scale squares of the color checker. **G** – green channel; **LED** – RGB LED illuminator; **Laser** – laser illuminator; **SkIm** – SkImager, **Exp Ch20** – exposition adjusted to the value of the square (Ch20) of the color checker, **norm** – normalized data.

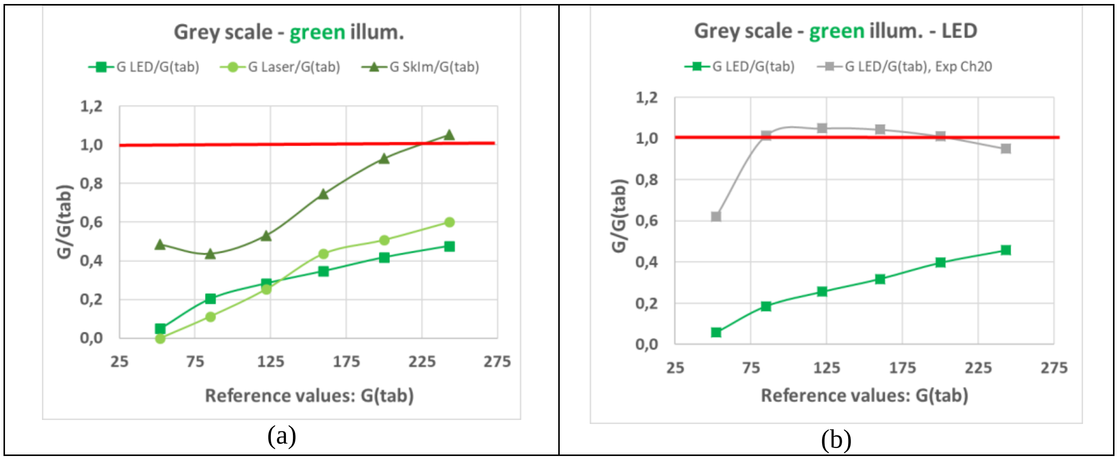

Fig.3. Comparison of the measured mean values and the reference (tabulated) values for the grey scale squares on the color checker. **G** – green channel; **LED** – LED illuminator; **Laser** – laser illuminator; **SkIm** – SkImager, **Exp Ch20** – exposition adjusted to the value of the square (Ch20) of the color checker, **norm** – normalized data.

3.2. Autofluorescence imaging

Under the 405 nm excitation, the detection wavelengths at 460+/-1 nm and 520+/-1 nm were selected to examine the autofluorescence (AF) contributions from NADH (τ_1 – short lifetime component) and FAD (τ_2 – long lifetime component), respectively. Comparison of the healthy and pathologic regions in the AF lifetime images of *ex-vivo* skin samples highlighted some differences in the "fast" and "slow" lifetime components τ_1 and τ_2, as presented in Table 2. One can see that the changes in τ_1 values are not significant while the changes of τ_2 are more pronounced at both registration wavelengths.

Table 2. Skin autofluorescence lifetime components at two detection wavelengths under 405 nm pulsed excitation.

Lifetime component	Detection wavelength 460 nm					
	Nevus	Skin	SCC	Skin	BCC	Skin
τ_1 (ns)	0,7-0,8	1,2-1,4	1-1,2	0,6-0,9	0,6-1,2	0,9-1,2
τ_2(ns)	3,5-4	5-6	5-6	3,5-4,5	4,5-6,5	4-5
	Detection wavelength 520 nm					
	Nevus	Skin	SCC	Skin	BCC	Skin
τ_1 (ns)	0,5-0,7	0,8-1	0,5-1; 3,5	0,5-1	0,5-1	0,5-1
τ_2(ns)	3,5-4,5	5-6	5,5-6	3,5-4,5	4,7-6	4-5

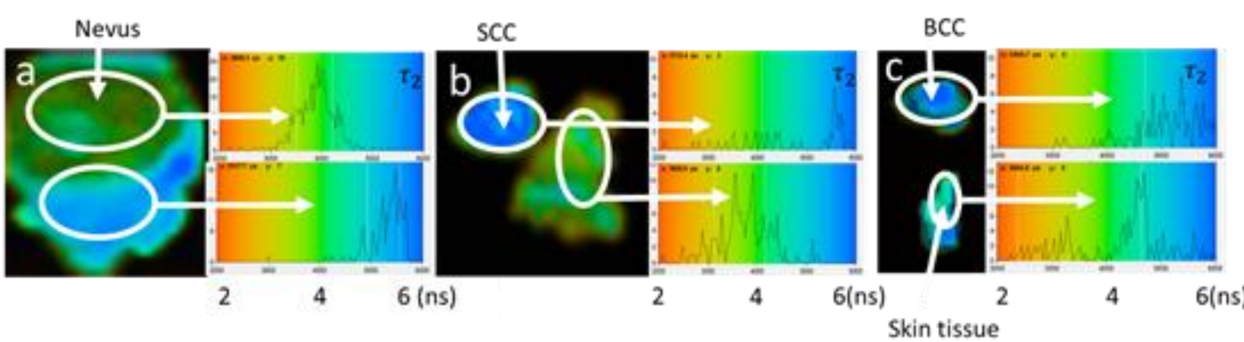

Fig.4. The distributions of τ_2 values at 520 nm for pathologic and healthy skin areas of three *ex-vivo* samples.

The 520 nm autofluorescence data seem to be most interesting – both malignant tumors (SCC and BCC) exhibited higher τ_2 values to compare with the surrounding healthy skin, while the τ_2 value for the common pigmented nevus was lower. It is illustrated on Figure 4 where the RoI's for each skin malformation are presented on the left and the distributions of the τ_2 values over the image pixels – on the right. In all cases the τ_2 values for the healthy and pathologic regions are clearly separated. Eventually, this feature may be exploited in future for skin tumor diagnostics.

3.3. Raman spectra

Figure 5 summarizes the Raman spectra *ex vivo* from healthy skin, SCC and BCC. The Raman spectra of skin display partially overlapped bands at 1440 – 1450 cm^{-1}, with contribution of lipids (CH2/CH3 bands from triolein and ceramide) and protein rich components (collagen, elastin and keratin) being specific to CH bending, CH stretching or asymmetric deformation modes. The 1300 cm^{-1} band also represent CH2 twisting and wagging modes in lipids (triolein). Lipids and proteins also have partially overlapping Raman spectral bands at 1650 – 1660 cm^{-1}, assigned to C–O stretching vibration of amide-I and C=C lipid stretch. Other characteristic Raman spectral features of collagen, elastin and keratin arise from amide-III α-helix conformation, C–N stretching, N–H (in plane) bending at 1269 cm^{-1}. Amide-III β sheet conformations contribute to a shoulder at 1248 cm^{-1} and C-C vibration of phenyl ring are detected at 1003 cm^{-1}. The peaks at 1063, 1080 cm^{-1} and 1128 cm^{-1} characterize the C–C skeletal stretching in lipids. The former mentioned lipids (triolein and ceramide) are also the major components of skin epidermal surface. Ceramide comprises half of the lipids in *stratum corneum* and triolein is found within the sebaceous glands[15].

The spectra of skin samples with BCC and SCC exhibited the loss of Raman major spectral bands (Fig. 5). Lowered concentration of triolein and collagen has been observed previously in skin cancer (SCC, BCC) by Feng et al[16]. Similarly, it has been shown by Nijsen et al.[17] that collagen is degraded by matrix metalloproteinases in BCC. Nevertheless, the presented Raman spectral peaks had not been reduced as much as in our study, implying even the relative increase in keratin or cell DNA specific bands for SCC or BCC.[16]

In vitro experiments, comparing Raman spectra of living and dead dc-3f cells, provided supplementary information on Raman spectral bands suppression related to changes in cell chemical components due to the shutdown of cell metabolism and the cell death (Fig. 6). We observed lower spectral intensity at 1645 cm^{-1} comprising the decrease of amide-I (1650 cm^{-1}), DNA bases (1576 cm^{-1}) and tryptophan (1616 cm^{-1}) Raman peak intensities[18]. In addition, dead cells also exhibit some decrease in the amount of cell membrane phospholipids (1065, 1244 cm^{-1}), the decreased amount of intracellular lipids (1450 cm^{-1}) and proteins (1083, 1450 cm^{-1}). Therefore, the observed significant decrease in Raman peak intensities might be also indicative for the extent of cell death within the solid tumors.

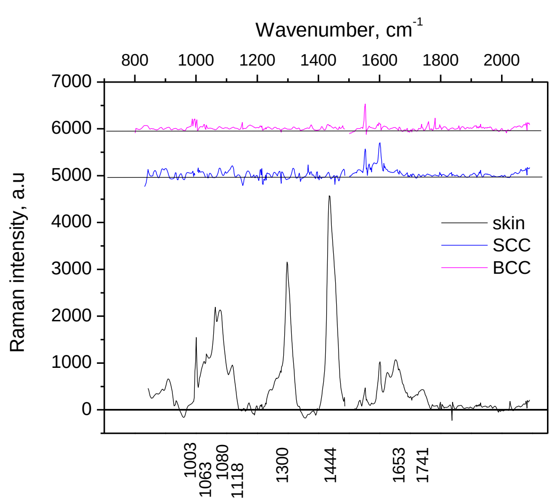

Fig. 5. Raman spectra for human healthy skin, SCC and BCC skin cancer *in situ*. Spectral resolution 0.17 nm, integration time 90 s, number of scans 1, slit width 50 μm. SCC and BCC spectra were offset for clarity.

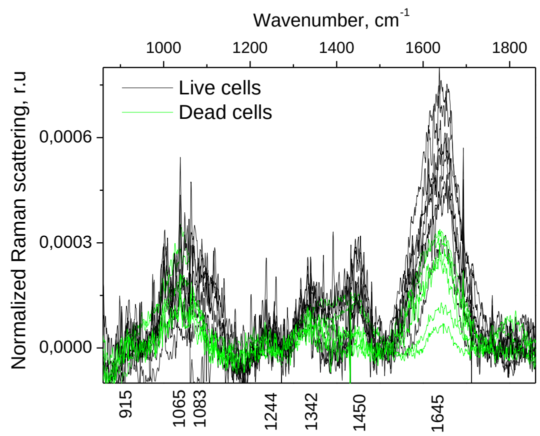

Fig. 6. Comparison of mean/area normalized Raman spectra for live dc-3f cells (black line) and dead cells (green line) from n=14 samples *in vitro*.

Several research groups recently applied Raman spectroscopy *ex vivo* for accurate classification of malignant tissue type.[3,20,21] However, in our study, the Raman spectra from BCC and SCC were mostly identical by the decreased amount of biochemical components, possessing only few low intensity spectral bands possibly ascribed to nucleobase (adenine and guanine) vibrations at 1578 cm^{-1} and amino acids (phenylalanine, tyrosine) vibrations at 1001 and 1607 cm^{-1} (Fig. 5). Nevertheless, the efficiency of pathological classification by conducting multimodal diagnostics can be more reliable. The improvement is likely based on detection of cellular metabolism shut down, resulting in altered concentrations of free NADH that can be identified by the shift of τ_1 component to a shorter lifetime. Such findings are not unexpected and are consistent with other group's results.[22,23]

4. SUMMARY

To summarize, results of the preliminary studies for development of tri-modal diagnostic imaging system confirm the potential of each modality for further exploitation. Some of the reported data indicate to possible new diagnostic applications in future – e.g. differences of the second autofluorescence lifetime components for benign and malignant skin lesions (3.2) and specifics of the Raman spectra related to living and dead cells (3.3). The combination of Raman and autofluorescence lifetime spectral measurements can provide complementary diagnostic criteria for diagnosis and classification of skin malformations.

ACKNOWLEDGEMENTS

This work was supported by the ERDF project #1.1.1.1/18/A/132 "Multimodal imaging technology for in-vivo diagnostics of skin malformations". Skin *ex-vivo* samples were provided in frame of the bilateral project for inter-academic exchange between between Latvian and Bulgarian Academies of Sciences "Multispectral and fluorescent imaging of skin tumours".

REFERENCES

[1] Lukinsone V., Veilande R., Plorina E.V., Kuzmina I., Bliznuks D., Boločko K., Derjabo A., Lihacova I., Spigulis J., "Multispectral and autofluorescence RGB imaging for skin cancer diagnostics", Proc.SPIE 11065, 110650A (2019).

[2] Zakharov V.P., Bratchenko I.A., Artemyev D.N., Myakinin O.O., Khristoforova Y.A., Kozlov S.V., Moryatov A.A., "Combined autofluorescence and Raman spectroscopy method for skin tumor detection in visible and near infrared regions," Clinical and Biomedical Spectroscopy and Imaging IV, Proc.SPIE 9537, 95372H (2015).

[3] Bratchenko I.A., Artemyev D.N., Myakinin O.O., Khristoforova Y.A., Moryatov A.A., Kozlov S.V., Zakharov V.P., "Combined Raman and autofluorescence *ex vivo* diagnostics of skin cancer in near-infrared and visible regions," J Biomed Opt 22(2), 27005 (2017).
[4] Morita S., Takanezawa S., Hiroshima M., Mitsui T., Ozaki Y., Sako Y. "Raman and autofluorescence spectrum dynamics along the HRG-induced differentiation pathway of MCF-7 cells," Biophys. J. 107(10), 2221-2229 (2014).
[5] Dochow S., Ma D., Latka I., Bocklitz T., Hartl B., Bec J., Fatakdawala H., Marple E., Urmey K., Wachsmann-Hogiu S., Schmitt M., Marcu L., Popp J. "Combined fiber probe for fluorescence lifetime and Raman spectroscopy," Anal.Bioanal.Chem. 407(27), 8291-8301 (2015).
[6] Dochow S., Fatakdawala H., Phipps J.E., Ma D., Bocklitz T., Schmitt M., Bishop J.W., Margulies K.B., Marcu L., Popp J., "Comparing Raman and fluorescence lifetime spectroscopy from human atherosclerotic lesions using a bimodal probe," J.Biophot. 9(9), 958-966 (2016).
[7] Wightman R., Busse-Wicher M., Dupree P., "Correlative FLIM-confocal-Raman mapping applied to plant lignin composition and autofluorescence," Micron 126, 102733 (2019).
[8] Majumder S.K., Keller M.D, Boulos F.I., Kelley M.C., Mahadevan-Jansen A., "Comparison of autofluorescence, diffuse reflectance, and Raman spectroscopy for breast tissue discrimination," J.Biomed.Opt. 13(5), 054009 (2008).
[9] Kuzmina I., Lacis M., Spigulis J., Berzina A., Valaine L., "Study of smartphone suitability for mapping of skin chromophores, J.Biomed.Opt., 20(9), 090503 (2015).
[10] Spigulis J., Oshina I., Berzina A., Bykov A., "Smartphone snapshot mapping of skin chromophores under triple-wavelength laser illumination", J.Biomed.Opt., 22(9), 091508 (2017).
[11] Ferulova I., Lihachev A., Spigulis. J, "Photobleaching effects on *in-vivo* skin autofluorescence lifetime," J.Biomed.Opt., 20(5), 051031 (2015).
[12] Diebele I., Kuzmina I., Lihachev A., Spigulis J., Kapostinsh J., Derjabo A., Valaine L., "Clinical evaluation of melanomas and common nevi by spectral imaging," Biomed.Opt.Express, 3(3), 467-472 (2012).
[13] Spigulis J., Rubins U., Kviesis-Kipge E., Rubenis O., "SkImager: a concept device for *in-vivo* skin assessment by multimodal imaging", Proc.Est.Acad.Sci., 63(3), 213-220 (2014).
[14] Spigulis J., Lihachev A., Lukinsone V., Osis M., Oshina I., "Lasers for *in-vivo* skin diagnostics: some recent developments", Proc. SPIE 11047, 1104703 (2019).
[15] Downing D.T., "Lipid and protein structures in the permeability barrier of mammalian epidermis," J. Lipid Res. 33(3), 301–313 (1992).
[16] Feng X., Moy A.J., Nguyen H.T., Zhang J., Fox M.C., Sebastian K.R., Reichenberg J.S., Markey M.K., Tunnell J.W., "Raman active components of skin cancer," Biomed.Opt.Exp. 8(6), 2835-2850 (2017).
[17] Nijssen A., Bakker Schut T.C., Heule F., Caspers P.J., Hayes D.P., Neumann M.H., Puppels G.J., "Discriminating basal cell carcinoma from its surrounding tissue by Raman spectroscopy," J.Invest.Dermatol. 119(1), 64-69 (2002).
[18] Wang H., Tsai T.H., Zhao J., Lee A.M., Lo B.K., Yu M., Lui H., McLean D.I., Zeng H., "Differentiation of HaCaT cell and melanocyte from their malignant counterparts using micro-Raman spectroscopy guided by confocal imaging," Photodermatol.Photoimmunol.Photomed. 28(3), 147-152 (2012).
[19] Sigurdsson S., Philipsen P.A., Hansen L.K., Larsen J., Gniadecka M., Wulf H.C., "Detection of skin cancer by classification of Raman spectra," IEEE Trans.Biomed.Eng. 51(10), 1784-1793 (2004).
[20] Bodanese B., Silveira F. L., Zângaro R. A., Pacheco M. T., Pasqualucci C. A., Silveira L. Jr., "Discrimination of basal cell carcinoma and melanoma from normal skin biopsies in vitro through Raman spectroscopy and principal component analysis," Photomed.Laser Surg. 30(7), 381-387 (2012).
[21] Lui H., Zhao J., McLean D., Zeng H., "Real-time Raman spectroscopy for *in vivo* skin cancer diagnosis," Cancer Res. 72(10), 2491-2500 (2012).
[22] Datta R., Heylman C., George S.C., Gratton E., "Label-free imaging of metabolism and oxidative stress in human induced pluripotent stem cell-derived cardiomyocytes," Biomed.Opt.Expr. 7(5), 1690-1701 (2016).
[23] Skala M.C., Riching K.M., Gendron-Fitzpatrick A., Eickhoff J., Eliceiri K.W., White J.G., Ramanujam N., "*In vivo* multiphoton microscopy of NADH and FAD redox states, fluorescence lifetimes, and cellular morphology in precancerous epithelia," Proc.Natl.Acad.Sci. USA 104(49), 19494–19499 (2007).